Available online at www.sciencedirect.com
SCIENCE DIRECT®
Physica D 206 (2005) 94–108
PHYSICA D
www.elsevier.com/locate/physd

Bubbling bifurcation: Loss of synchronization and shadowing breakdown in complex systems

R.L. Viana[a,*], C. Grebogi[b,c], S.E. de S. Pinto[a,d], S.R. Lopes[a], A.M. Batista[d], J. Kurths[c]

[a] *Departamento de Física, Universidade Federal do Paraná, 81531-990, Curitiba, Paraná, Brazil*
[b] *Instituto de Física, Universidade de São Paulo, 05315-970, São Paulo, São Paulo, Brazil*
[c] *Institut für Physik, Lehrstuhl Nichtlineare Dynamik, Universität Potsdam, PF 601553, D-14415 Potsdam, Germany*
[d] *Departamento de Matemática e Estatística, Universidade Estadual de Ponta Grossa, Ponta Grossa, Paraná, Brazil*

Received 10 February 2004; received in revised form 16 February 2004; accepted 3 May 2005
Available online 23 May 2005
Communicated by C.K.R.T. Jones

Abstract

Complex dynamical systems with many degrees of freedom may exhibit a wealth of collective phenomena related to high-dimensional chaos. This paper focuses on a lattice of coupled logistic maps to investigate the relationship between the loss of chaos synchronization and the onset of shadowing breakdown via unstable dimension variability in complex systems. In the neighborhood of the critical transition to strongly non-hyperbolic behavior, the system undergoes on–off intermittency with respect to the synchronization manifold. This has been confirmed by numerical diagnostics of synchronization and non-hyperbolic behavior, the latter using the statistical properties of finite-time Lyapunov exponents.

Keywords: Bubbling bifurcation; Synchronization; Shadowing breakdown

1. Introduction

The study of collective spatio-temporal behavior in complex system has received a great deal of attention over the last 20 years or so. It is widely agreed that a complex system should fulfill the following properties: (i) they are composed of many parts interrelated in a nontrivial manner; (ii) they can exhibit both ordered and random behaviors; and (iii) they display a hierarchy of structures over a wide range of lengths [1]. Spatially extended systems built from coupled chaotic maps or flows typically belong to the category of complex systems, for different parts of the lattice can exhibit different dynamics, say, regular and chaotic, forming structures where coherent and incoherent behavior coexist [2]. There are many quantitative ways to characterize the complexity of a given system, more effectively being a mix of sundry

* Corresponding author. Tel.: +55 41 3613098; fax: +55 41 3613418.
E-mail address: viana@fisica.ufpr.br (R. Viana).

0167-2780/$ – see front matter © 2005 Elsevier B.V. All rights reserved.
doi:10.1016/j.physd.2005.05.001

numerical diagnostics like the Lyapunov spectrum, the Kolmogorov–Sinai entropy, the Fisher information, and so on [3]. In addition, there are also several non-traditional measures of complexity, based on symbolic dynamics and a renormalized entropy [4].

Synchronization has been one of the collective phenomena most intensively studied, mainly after the discovery that chaotic systems, in spite of their natural instability, can synchronize their trajectories [5,6]. While a considerable amount of research has focused on small assemblies of coupled systems, the question of how and why complex systems with many degrees of freedom synchronize still presents challenging questions [7]. Synchronization results in a system as the outcome of the competition between two antagonistic factors: the intrinsic disorder caused by the nonlinear behavior of each system unit and the diffusive effect provoked by their coupling [8,9]. When the latter dominates the former, as in many global coupling schemes, the entire system (or portions of it) can synchronize, meaning that the state variables for neighbor units share a common value [9]. On the other hand, local couplings are such that the diffusive effect typically is not able to surpass the intrinsic randomness and, as a result, synchronization is not achieved [10].

There is considerable evidence that synchronization occurs as a well-defined transition for a given strength of the coupling effect [8]. The vicinity of the critical point for transition to chaos synchronization is characterized by an intermittent behavior, in which the synchronized dynamics is interrupted by chaotic bursts. This fact has been previously reported for lattices of coupled piecewise linear chaotic maps [11]. The chaotic bursting accompanying the synchronization transition is an example of the so-called on–off intermittency [12].

The rationale for explaining the presence of on-off intermittency lies in the transversal dynamics to the synchronization manifold whenever it exists in the high-dimensional phase space of the coupled system [13]. When this manifold becomes transversally unstable, there are consequences in terms of the synchronized properties of chaotic trajectories [14]. There is also a profound change in the dynamics of the synchronization manifold after it loses transversal stability, since the synchronized dynamics becomes non-hyperbolic via a mechanism called unstable dimension variability [15–17]. It is characterized by the breakdown of the continuous splitting between stable and unstable manifolds, because the dimension of the unstable and stable eigenspaces vary along the chaotic invariant set [18]. The consequences of unstable dimension variability are disastrous from the point of view of the shadowing of the numerically generated chaotic trajectories [19–22].

The relation between loss of synchronization and the properties of the Lyapunov spectrum has been previously investigated in a lattice of coupled maps [11]. In this paper, we extend this approach to put into evidence the connection between the collective phenomena and the chaotic bursting which leads to shadowing breakdown. The key point we wish to convey is that the transition to synchronization in the coupled map lattice is accompanied by the loss of transversal stability of the synchronization manifold, and the consequent shadowing breakdown of chaotic trajectories by means of unstable dimension variability. Moreover, as a result of unstable dimension variability, there appears a chaotic bursting in the vicinity of the synchronization transition which is in fact a case of on–off intermittency [23]. These claims are supported by strong numerical evidence which uses diagnostics of nonhyperbolicity and synchronization for the loss of hyperbolicity via unstable dimension variability. While the topics treated in this paper, like shadowing breakdown, loss of synchronization, and on–off intermittency, have been intensively studied for their own, this work aims to clarify links between them, focusing on different numerical techniques employed to identify their occurrence in a dynamical system.

The structure of this paper is as follows. In Section 2 we present the paradigmatic spatially extended system to be studied, and the characterization of chaotic dynamics for it. Section 3 considers the existence of completely synchronized states for the lattice. Section 4 analyzes chaotic bursting accompanying the loss of synchronization as an on–off intermittent situation, and deals with the definition and characterization of phase synchronization for the system. The synchronization problem, analyzed from the point of view of shadowing breakdown, is considered in Section 5, which also studies the evolution of unstable dimension variability as a system parameter is varied. Numerical evidence of unstable dimension variability is provided by computing finite-time exponents. Our conclusions are left to the final section.

2. Logistic map lattice with a power-law coupling

Coupled map lattices are widely reckoned as simple but paradigmatic models for complex systems like neural networks, excitable media, oscillator chains, etc. [2]. They present both space and time as discrete variables, while retaining a continuous state variable that is capable to undergo a smooth nonlinear dynamics. We examine, in particular, a one-dimensional chain of N coupled logistic maps at outer crisis $x \mapsto f(x) = 4x(1-x)$, where $x_n^{(i)} \in [0,1]$ represents the state variable for the site i ($i = 1, 2, \ldots, N$) at time n. Our results, though, should not be quantitatively very different if we had chosen the logistic map parameter to be below the outer crisis value.

In this paper we use a variable range coupling in which the interaction strength between sites decays in a power-law fashion with the lattice distance [24–26]

$$x_{n+1}^{(i)} = (1-\epsilon) f(x_n^{(i)}) + \frac{\epsilon}{\eta(\alpha)} \sum_{j=1}^{N'} \frac{1}{j^\alpha} [f(x_n^{(i+j)}) + f(x_n^{(i-j)})], \quad (1)$$

where $\epsilon > 0$ and $\alpha > 0$ are the coupling strength and range, respectively, and $\eta(\alpha) = 2\sum_{j=1}^{N'} j^{-\alpha}$, with $N' = (N-1)/2$ for N odd. We use periodic boundary conditions for the lattice, or $x_n^{(i)} = x_n^{(i \pm N)}$.

The coupling prescription used in Eq. (1) is nonlocal since it connects maps from distant parts of the lattice. Such couplings are used in neural network architectures with local production of information [27,28], and they also result from discretization of some partial integro-differential equations modeling physico-chemical reactions [29]. Further applications are found in assemblies of biological cells with oscillatory activity, whose interaction is mediated by some rapidly diffusing chemical substance [30], and in systems of diffusive coupling in nucleation kinetics with elimination of the rapidly diffusing components [31]. Nonlocal prescriptions such as (1), for which the coupling intensity decays with the distance along the lattice in a power-law, have been used in models of some biological neural networks [32].

The virtue of the coupling prescription in Eq. (1) is that it allows one to pass continuously from a local Laplacian-type coupling [33]

$$x_{n+1}^{(i)} = (1-\epsilon) f(x_n^{(i)}) + \frac{\epsilon}{2} [f(x_n^{(i+1)}) + f(x_n^{(i-1)})], \quad (2)$$

obtained when $\alpha \to \infty$, to a global mean-field coupling [35,9]

$$x_{n+1}^{(i)} = (1-\epsilon) f(x_n^{(i)}) + \frac{\epsilon}{N-1} \sum_{j=1,\, j\neq i}^{N} f(x_n^{(j)}), \quad (3)$$

when $\alpha = 0$. Hence, as α increases, we shorten the effective coupling range and can investigate any phenomenon which depends on this effect. Such an example is chaos synchronization in coupled map lattices [8]. Short range (nearest-neighbor or diffusive) couplings do not favor synchronization, since the coupling effect is typically too weak to overcome the disorder caused by the extended map dynamics [33,34]. On the other hand, nonlocal couplings tend to facilitate synchronization, since the coupling effect extends throughout the lattice, as in globally coupled map lattices, where each site interacts with the mean field produced by all the other ones [35,36].

The uncoupled logistic maps, at outer crisis, have the Lyapunov exponent $\lambda_U = \ln 2$ for almost all initial conditions x_0 (except for a Lebesgue measure zero set of points). On the other hand, the coupled map lattice (1) exhibits a Lyapunov spectrum consisting of N ordered exponents $\lambda_1 = \lambda_{\max} \geq \lambda_2 \geq \cdots \lambda_N$. Since we expect that many of these exponents be positive, a quantity of interest is the density of the Kolmogorov–Sinai entropy. We depict in Fig. 1 its dependence with the parameters characterizing the coupling intensity – its strength ϵ and range α – for the dynamical model given by Eq. (1). For a global coupling ($\alpha = 0$), the mean value of the entropy density is close to zero for strong coupling (large ϵ) and, beyond a given critical value $\alpha \approx 0.2$, it grows monotonically until it reaches a maximum value, achieved for vanishing coupling, which turns out to be just the Lyapunov exponent for uncoupled maps $\lambda_U \approx 0.69$.

As the effective range α further increases, we still have such a transition, but it becomes delayed and not so sharp, with the presence of an oscillatory behavior of increasing amplitude as ϵ decreases. As ϵ goes to zero, it eventually has the same steep and monotonic increase characteristic of global couplings. When α is large, the

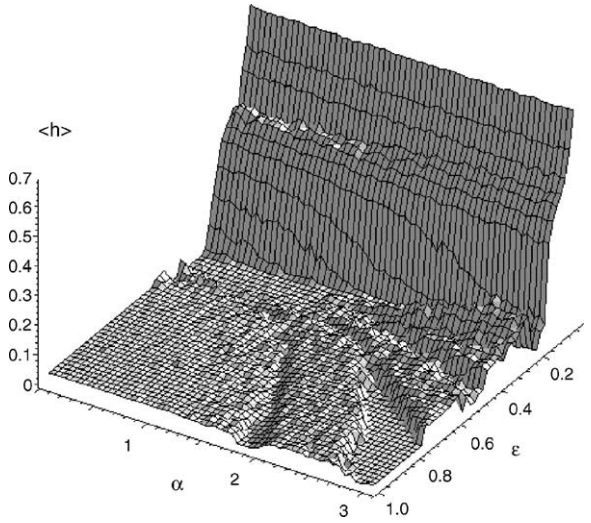

Fig. 1. Kolmogorov–Sinai entropy of the coupled map lattice (1) vs. coupling strength and range, for $N = 21$.

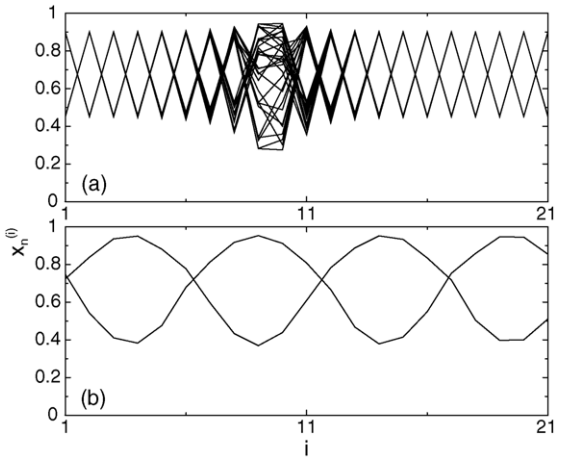

Fig. 2. Overlap of 30 lattice patterns for $N = 21$ coupled maps with $\alpha = 3.0$ and (a) $\epsilon = 0.165$; (b) $\epsilon = 0.950$.

coupling between maps becomes effectively noticeable only with the nearest neighbors, and even a strong coupling is not able to change the global chaotic dynamics of the orbits, although the number of positive Lyapunov exponents diminishes as the coupling strength grows. The numerical features we have observed agree with analytical expressions for the Lyapunov spectrum of power-law lattices such as Eq. (1) [37].

When both α and ϵ have large values, i.e. for strong and essentially local coupling, the entropy is low (Fig. 1) which may be explained as a result of a chaos suppression mechanism by pattern selection. Fig. 2(a) shows, for $\alpha = 3.0$ (the upper limit of the range depicted in Fig. 1), an overlap of 30 lattice patterns, after we have waited 10,000 transient iterations. The resulting zig-zag pattern is dominant over the lattice, with exception of a defect, where the dynamics is apparently chaotic. The resulting entropy is nonzero, yet very small. In general, for a frozen random pattern, there is a decrease of the entropy with increasing nonlinearity [38]. For slightly higher ϵ (Fig. 2(b)), however, there is complete selection of a period-2 pattern with zero entropy, for there is no positive Lyapunov exponent. This is in accordance with the conjecture that a pattern selection occurs with smaller Lyapunov exponent. Patterns with higher Lyapunov exponents, like the ones exhibiting defects such as in Fig. 2(a), tend to collapse under the influence of their neighbors to a pattern with smaller Lyapunov exponent (the *zig-zag* patterns) [38].

The coupled map lattice treated herewith has the characteristics necessary to be classified as a bona fide complex system [1,3] since: (a) it is composed by many parts, represented by the coupled maps, which interact according to a well-defined prescription; (b) there is coexistence among ordered and random behaviors, as illustrated by Fig. 2(a); and (c) we can devise a hierarchy among coexistent structures. The latter issue will be clarified later on in this work, when we classify patterns related to synchronized behavior and find a power-law distribution for the corresponding typical lengths.

3. Chaos synchronization in the coupled map lattice

Synchronization of chaotic dynamics in coupled systems became, in the past decade, the convergence point of many analytical and numerical techniques of analysis [7]. Besides its own interest, as a collective spatio-temporal phenomenon, synchronization in coupled maps and oscillators have applications in arrays of Josephson junctions [39–41], assemblies of flashing fireflies [42], chaotic laser arrays [43], and physiological systems [44], among others.

Complete synchronization of a coupled map lattice means the existence of identical sites with

same values for the state variables at a given time n: $x_n^{(i)} = x_n^{(i+1)} = x_n^{(i+2)} = \cdots x_n^{(i+N_j)}$. If $N_j = N$, the entire lattice is synchronized. Otherwise one has a synchronization cluster of length N_j. The phase-space is N-dimensional, but a completely synchronized state lies in a one-dimensional synchronization manifold $\mathcal{S}$. All the $N-1$ remaining directions are referred to as transversal directions. If the synchronized state is chaotic it follows that $\lambda_{\max} > 0$, and the stability of the synchronization manifold is thus determined by the $N-1$ remaining transversal Lyapunov exponents. If $\lambda_2 > 0$ (the second exponent) then $\mathcal{S}$ is transversally unstable, and the synchronized state is unlikely to occur for typical initial conditions in phase space.

To consider the amplitude synchronization of the lattice, we resort to a numerical diagnostic provided by the complex order parameter introduced by Kuramoto [45], and here adapted for coupled map lattices as [26]

$$z_n = R_n \exp(2\pi i \varphi_n) \equiv \frac{1}{N} \sum_{j=1}^{N} \exp(2\pi i x_n^{(j)}), \qquad (4)$$

where R_n and φ_n are the amplitude and angle, respectively, of a centroid phase vector (for a one-dimensional chain with periodic boundary conditions). A time-average $\overline{R} = \lim_{M\to\infty}(1/M)\sum_{n=0}^{M} R_n$ is computed over an interval large enough to warrant that the asymptotic state has been achieved by the lattice. Moreover, we also consider an average value of $\overline{R}$ over five different and randomly chosen initial conditions.

The combination of strong coupling and small range produces a plateau near unity in plots of the order parameter magnitude $R(n)$, indicating complete synchronization, like in the globally coupled case (Fig. 3(a)). This follows from the coherent superposition of the phase vectors with the same amplitude at each time for all lattice sites. Fixing the coupling strength and increasing the effective range, we find that the synchronization plateau begins to breakdown through intermittent spiking (Fig. 3(b)). As the effective range is further increased these spikes become more frequent and the order parameter magnitude can have lower values (Fig. 3(c)). On the other hand, if the maps were uncoupled ($\epsilon = 0$), we would expect a pattern with site amplitudes $x_n^{(j)}$ so spatially uncorrelated that they might be considered essentially as random variables. In this case, the order parameter z_n, being a space average of terms

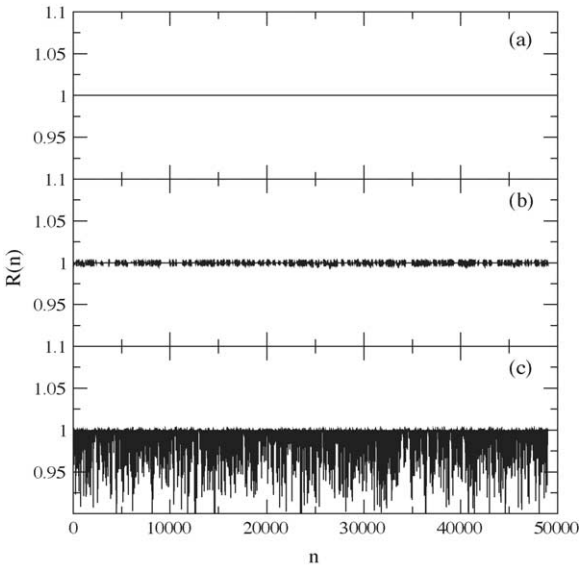

Fig. 3. Time series of order parameter magnitude $R(n)$ for a coupled logistic map lattice defined by Eq. (1), with $N = 21$, $\epsilon = 1.0$ and (a) $\alpha = 1.0483$, (b) 1.1483, and (c) 1.1583.

of the form $e^{2\pi i x_n^{(j)}}$, would nearly vanish at each time. As the coupling strength grows, diffusion adds spatial correlations to the site amplitudes, and the summation in Eq. (4) becomes nonzero, increasing nonlinearly with ϵ.

Let us investigate now the dependence of the average order parameter magnitude $\overline{R}$ on the quantities characterizing coupling (strength versus effective range) (Fig. 4(a)). In fact, for strong coupling and small effective range we have a completely synchronized chaotic lattice since, by comparing with Fig. 1, we have large values for the entropy. This large plateau suffers a breakdown to a situation with weak or no synchronization at all, through a steep ramp with irregular spikes for small coupling and large effective range. This is best viewed in a projection (Fig. 4(b)), where we separate regions with: (i) synchronized chaotic orbits; (ii) a transitional regime; and (iii) completely non-synchronized orbits [46]. These regions are bounded by the curves $\epsilon^*(\alpha)$ and $\epsilon_c(\alpha)$. The marked points of the former curve correspond to values of ϵ^* and α for which the average order parameter magnitude $\overline{R}$ ceases to be equal to the unity. The points on the curve $\epsilon_c(\alpha)$ were computed by means of the finite-time Lyapunov exponents, as will be explained in Section 7. The curves themselves

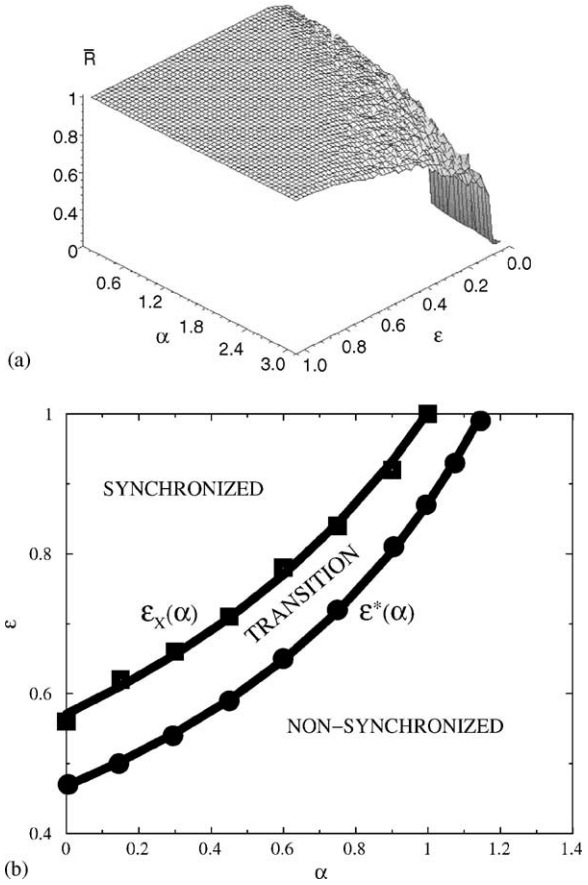

Fig. 4. (a) Time-averaged order parameter magnitude $\bar{R}$ vs. coupling strength and effective range; (b) projected view showing the synchronization regions. The solid curves correspond to nonlinear fittings.

in 4(b) are nonlinear fittings of the form $1/(a - b\alpha)$, where $a = 2.14$ and $b = 0.995$ for the $\epsilon^*(\alpha)$ curve; and $a = 1.75$ and $b = 0.754$ for the $\epsilon_c(\alpha)$ one.

By fixing the parameter range at an intermediate value, say $\alpha = 0.4$, and decreasing the coupling strength ϵ from its maximum value to be considered in this paper, 1.0, to zero, the following happens. For ϵ large enough we have $\bar{R} = 1$, or a completely synchronized chaotic state. When $\epsilon = \epsilon_c(0.4) \approx 0.69$ it starts to be interrupted by intermittent bursts of non-synchronized behavior, but eventually the stationary completely synchronized regime is achieved. The bursting becomes more frequent as the coupling strength is further decreased and, at $\epsilon = \epsilon^*(0.4) \approx 0.57$, the order parameter vanishes and the lattice becomes non-synchronized, never to achieve a completely synchronized state. Hence, the interval $\epsilon_c < \epsilon < \epsilon^*$ characterizes a transition region for which the intermittent bursting is a transient phenomenon.

This scenario is robust and present for a large portion of the coupling parameter plane. As we increase the value of the effective range parameter α from zero, it turns out that the interval characterizing a transition region is pushed towards higher values of the coupling strength ϵ. We can understand this hysteresis since the higher the effective range α is, the closer we are to a locally coupled lattice, in which only the nearest neighbors contribute in a significant way. It becomes then increasingly more difficult to have a stationary completely synchronized state. We call $\alpha_c \approx 0.940$ the range parameter value for which the first critical curve reaches the upper limit given by $\epsilon_c(\alpha_c) = 1$. Accordingly, $\alpha^* \approx 1.146$ is the value where the second critical curve is such that $\epsilon^*(\alpha^*) = 1$. Hence, for $\alpha > \alpha^*$, we do not observe a stationary complete synchronization state, irrespective of how strong the coupling may be, i.e. the intermittent bursting continues for an arbitrarily long time.

We find that the critical range parameter necessary for chaotic synchronization, or α^*, depends on the lattice size, diminishing as we increase the number of coupled maps (Fig. 5). We obtained that a power law fits well this finite-size scaling

$$\alpha^*(N) \sim \exp[(\ln N)^{-\tilde{\gamma}}], \tag{5}$$

where $\tilde{\gamma} = 1$, up to the numerical accuracy. In this way, it is possible to get a value of $\alpha^*_\infty \approx 0.44$ in the $N \to \infty$.limit.

These results are compatible with the assumption that a globally coupled lattice favors synchronization due to the long-range spreading of the interactions. In the limit of vanishing α, the coupling is such that each site interacts with the mean field of other sites. Any tendency to synchronize is transmitted to all other maps, regardless of their relative distance along the lattice. On the other hand, a locally coupled lattice connects the nearest neighbors of a given site, and this is an obstacle to synchronization. Disturbances do slowly move along the lattice, and this diffusive effect is easily surpassed by the intrinsic randomness present in the chaotic dynamics of each site.

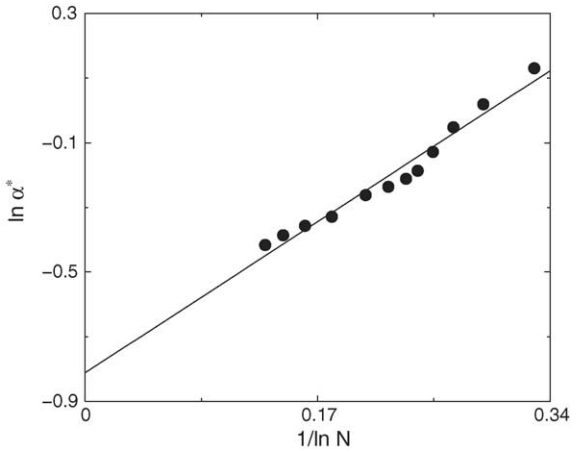

Fig. 5. Dependence of the critical range parameter on the lattice size for chaotic synchronization, for $\epsilon = 1.0$.

4. Intermittent transition to synchronization

The transition from a synchronized to non-synchronized behavior, in coupled map lattices, has many features common to structural phase transitions [47]. In the vicinity of the critical point, for example, an Ising system is expected to present fluctuations in the corresponding order parameter, which is the magnetization. Coupled map lattices, which have the Kuramoto's order parameter, also do present such fluctuations. They are manifested as intermittent bursts which, as we shall see, have the universal features of the on–off intermittency.

Let us focus our attention on Fig. 4(b), where a representative portion of the phase diagram, using the Kuramoto's order parameter, is shown. Near the critical curve $\epsilon^*(\alpha)$, the time series of the order parameter magnitude presents laminar regions, a fact already observed in other coupled map lattices [11]. The laminar regions of synchronization presented in Fig. 3 have typically different lengths τ_i, having an exponential distribution, but their average length is found to obey a power-law scaling with the difference $\alpha - \alpha^*$, for $\alpha \gtrsim \alpha^*$: (Fig. 6):

$$\langle \tau \rangle = \frac{1}{N_\mathrm{p}} \sum_{i=1}^{N_\mathrm{p}} \tau_i \sim (\alpha - \alpha^*)^{-\gamma}, \quad \text{for} \quad \alpha \to \alpha^*, \quad (6)$$

with $\gamma = 1/2$, within the numerical accuracy. This suggests that the transition to synchronization occurs through a crisis [48].

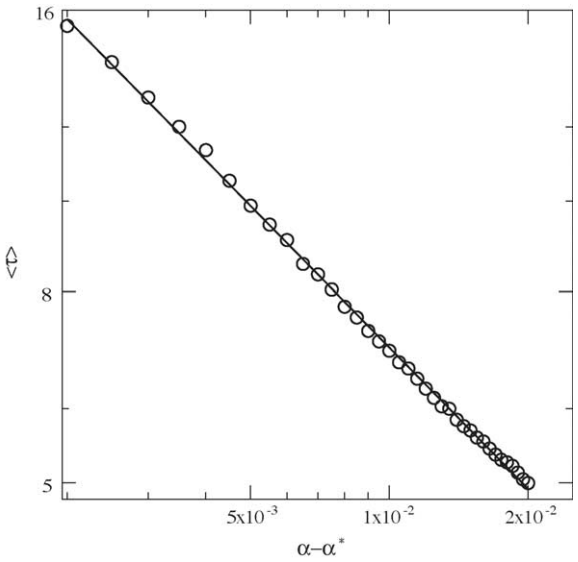

Fig. 6. Average length of the synchronization plateaus vs. $\alpha - \alpha^*$ for $\epsilon = 1.0, \alpha^* = 1.1463177$. The solid line is a power law least-squares fit with exponent 0.502.

The rationale for this analogy is the identification of the bursts between laminar regions as a kind of chaotic transient, similarly to that occurring when a chaotic attractor suffers a crisis by collision with an unstable periodic orbit. The average chaotic transient length in one-dimensional maps, like the logistic map $f(x) = rx(1-x)$ at $r = 4$, obeys a scaling identical to (6), with the same critical exponent. In two-dimensional maps this exponent is related to the stable and unstable eigenvalues of the unstable periodic orbit with which the chaotic attractor collides.

In ref. [49] there was considered a boundary crisis in a two-dimensional map with an invariant subspace in which a chaotic orbit lies. The dynamics in the transversal direction is such that there is another attractor at infinity. For a given range of a system parameter there is a fractal basin boundary between the basins of the chaotic and the infinity attractor. As the system parameter approaches a critical value, this basin boundary collides with the chaotic attractor in an infinitely large number of points. Each unstable point suffers a saddle-repeller bifurcation, in which the saddle belonging to the chaotic attractor in the invariant subspace coalesce with the repeller lying in the fractal basin boundary. This has been called an unstable-unstable pair bifurcation [50,51].

This analogy can be pushed forward if we consider that the chaotic attractor lies in the synchronization manifold (when the maximal Lyapunov exponent is positive, $\lambda_1 > 0$), which is itself an invariant manifold of the coupled map lattice (1) [52]. Hence, the transition to synchronization is mediated by an unstable-unstable pair bifurcation occurring in the synchronization manifold, in which a saddle loses its transversal stability. This fact will be exploited in the next section, where we consider the onset and evolution of shadowing breakdown in such a system.

Another distinctive feature of the intermittent transition to synchronization is the universal character of the statistics of the laminar regions [53]. In Fig. 7(a) we present a histogram for the length of the laminar regions. Two different regimes are highlighted: for shorter times, the histogram is well-fitted by a power-law $P(\tau) \sim \tau^{-\gamma}$, with $\gamma \approx 1.5$ (Fig. 7(b)); whereas the scaling is exponential $P(\tau) \sim \mathrm{e}^{-\kappa\tau}$ for larger times, with $\kappa \approx 10^{-3}$ (Fig. 7(c)).

This 3/2-scaling, for shorter τ, does not persist for other synchronization regions shown in the phase diagram of Fig. 4, as illustrated in Fig. 8. There we plot distributions obtained for $\epsilon = 0.7$ and $\epsilon = 0.4$, respectively below and above the critical transition to complete synchronization behavior. In this case we still have a power-law scaling, but with an exponent different from 3/2.

The presence of the 3/2-scaling plus the exponential decay indicates that on–off intermittency is taking

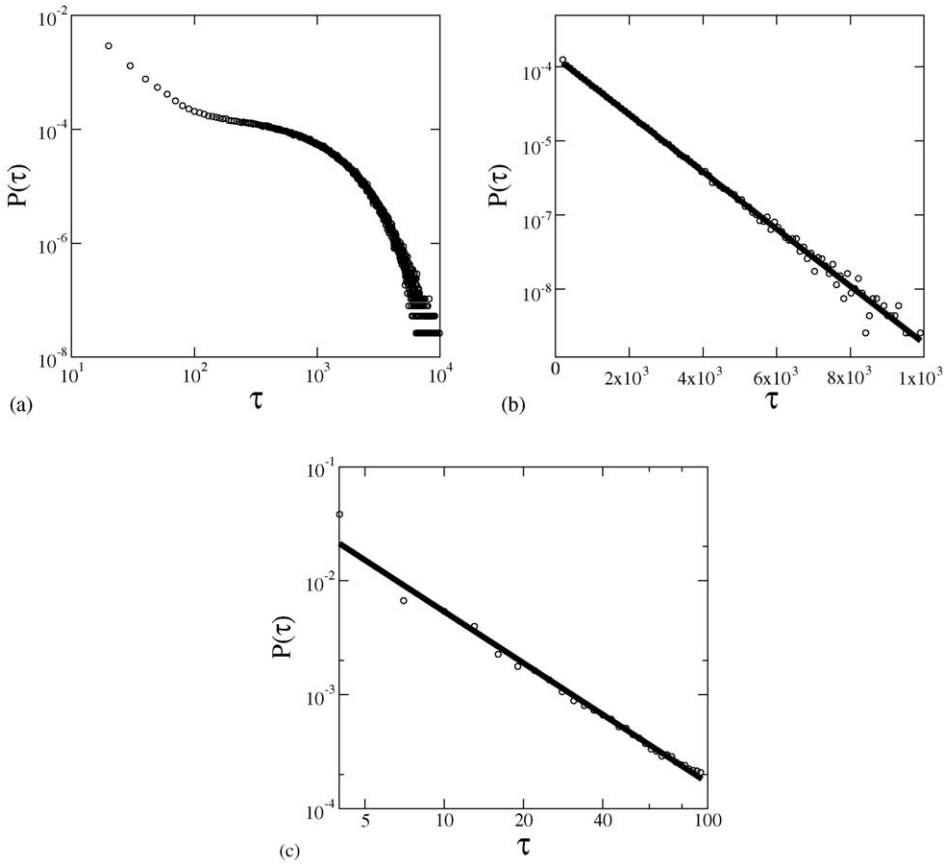

Fig. 7. (a) Histogram for the length τ_i of the synchronization plateaus; (b) magnification of the long time region, showing an exponential scaling law; (c) magnification of the short time region, showing a power-law scaling. The coupling parameters are $\epsilon = 1.0$, and $\alpha = 1.147$.

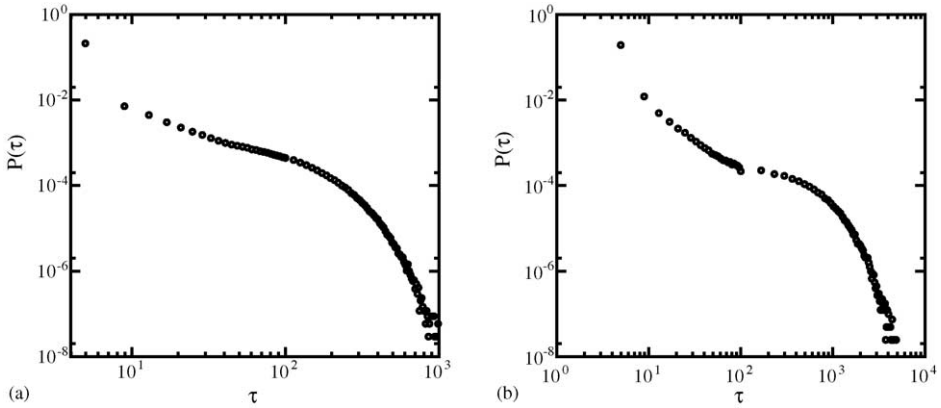

Fig. 8. Histogram for the length of the synchronization plateaus for $\alpha = 0.476$ and (a) $\epsilon = 0.7$; (b) $\epsilon = \epsilon^*(0) \approx 0.47$.

place in the transition to synchronization [12]. As a matter of fact, the transversal stability properties of the invariant synchronization manifold provide a support for this statement. In the transition region, trajectories off but very near the synchronization manifold experience intermittent bursting, such that numerical diagnostics using an insufficiently large time interval could erroneously point out the absence of complete synchronization [54,55]. The system is now in the neighborhood of an unstable-unstable pair bifurcation so different parts of the lattice are pulled away or towards the synchronization manifold, producing the sequence of bursting regions. The chaotic bursting on a portion of the lattice appears as random kicks on other parts due to the coupling. In fact, the existence of two scalings with a shoulder in between, as depicted in Fig. 7, indicates the presence of noise in the on–off intermittent scenario, with a crossover time proportional to the noise level.

There are many situations of physical interest in which two or more continuous-time oscillators may have different amplitudes, even in a chaotic regime, but with a well-expressed *phase coherence*. The oscillator phase can be defined in various ways for continuous-time systems, the simplest one being a geometrical phase for a bounded attractor [48,56]. For coupled map lattices, however, this procedure cannot be carried over, since there is no vanishing Lyapunov exponent which would enable an interaction of the coupled phases, in order to yield phase synchronization. Instead of phase synchronization, coupled maps can display a coherence with respect to the direction of their temporal evolution.

Direction-coherent maps are defined as those showing local maxima or minima for their amplitudes at the same time [57], such that the direction is provided by two sequential iterations of the coupled maps [58,59]. A lattice site $x_n^{(j)}$ thus has a direction at a fixed time n given by

$$P_n^{(j)} = \begin{cases} 1, & \text{if } x_n^{(j)}/x_{n-1}^{(j)} > 1, \\ 0, & \text{otherwise,} \end{cases} \tag{7}$$

in such a way that a direction-coherent cluster is a union of adjacent maps with the same value of $P_n^{(j)}$.

Fig. 9 shows the overlap of amplitude-site profiles, for a hundred successive times and after a large number of transients have decayed, for a lattice of strongly coupled logistic maps in the intermediate range situation. In order to allow for a better visualization of the local maxima and minima, we depict only three sequential profiles, where the arrows show the phase directions. On the basis of the previous definition we can say that between times $n = 1005$ and 1006 all sites in Fig. 9 are direction-coherent, whereas, between $n = 1006$ and $n = 1007$, this occurs just for a fraction (nearly half) of them.

We denote by $\mathcal{N}_n^{(0)} = \sum_{j=1}^{N}(P_n^{(j)} = 0)$ and $\mathcal{N}_n^{(1)} = \sum_{j=1}^{N}(P_n^{(j)} = 1)$ the number of lattice sites at a given time with phases equal to 0 and 1, respectively. We define a coherence ratio ρ_n as [58,59]

$$\rho_n \equiv \frac{1}{N}\max(\mathcal{N}_n^{(0)}, \mathcal{N}_n^{(1)}), \tag{8}$$

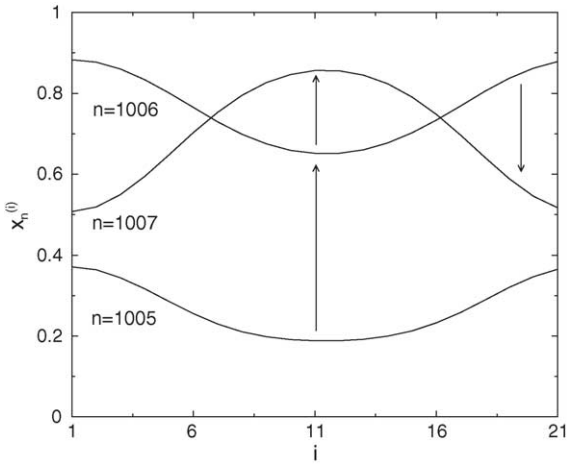

Fig. 9. Overlap of 3 space-amplitude plots for a lattice, after 1004 transients, of $N = 21$ maps with $\alpha = 0.49$, and $\epsilon = 1.0$. The arrows indicate the phase direction.

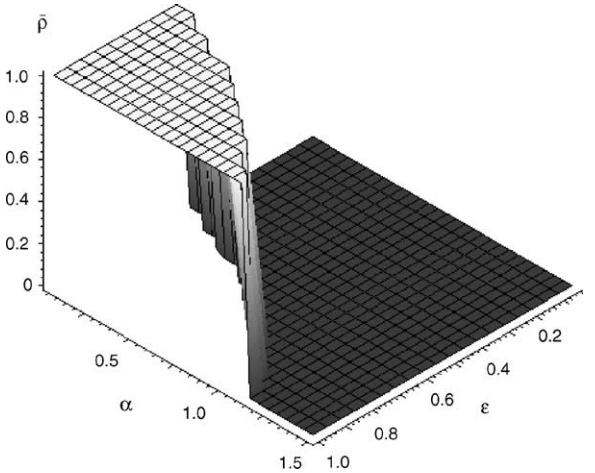

Fig. 11. Time-averaged direction-coherence ratio as a function of the coupling strength and range for $N = 21$ coupled logistic maps.

in such a way that, if the directions of all lattice sites flip randomly between 0 and 1, the ratio would approach a constant value, whereas if $\rho = 1$ all lattice sites are direction-coherent (Fig. 10(a)). The minimum value for this ratio is $\rho = 1/2$, a situation in which half of the sites have $P_n^{(j)} = 0$.

As the lattice pattern evolves with time, this ratio varies in an intermittent fashion, as illustrated by Fig. 10(b). The coherence ratio has laminar phases at 1.0 with irregular bursts, some of them approaching the lower bound at $\rho = 1/2$ [Fig. 10(c)], indicating an intermittent behavior very similar to that described in the previous section for amplitude synchronization. The average duration of the laminar intervals scales with the range parameter in a power-law fashion, just like that depicted in Fig. 6. Fig. 11 shows the dependence of the time-averaged coherence ratio $\bar{\rho} = \lim_{M\to\infty}(1/M)\sum_{n=0}^{M}\rho_n$, which compares well with Fig. 4(a), where the time-averaged order parameter is plotted against the same parameters. In particular, the $\epsilon^*(\alpha)$ curve in Fig. 4(a), which indicate the loss of complete synchronization of chaos, and the corresponding curve in 11, which signals loss of direction coherence, nearly coincide. This occurs because, while complete synchronization obviously implies direction coherence, the converse is not necessarily true, as illustrated by Fig. 9, where we see that the maps, though not complete synchronized, have a direction coherence. This difference is manifested mainly in the transitional region of intermittent transition to complete synchronization, which is very narrow in Fig. 11 compared with that observed in the order parameter results of Fig. 4(a). Moreover, we have numerically verified that the number of coherence-direction ratio laminar intervals also depends on the interval lengths according to a power-law distribution, just like that observed in Fig. 7. In a lattice of piecewise linear maps the slope of the corresponding linear fit is close to the 3/2-value characteristic of on–off intermittency [11].

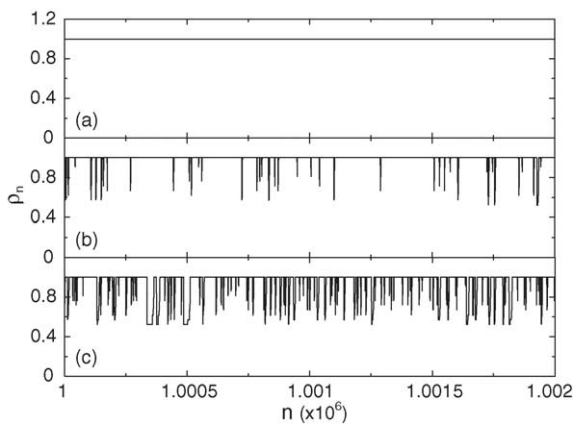

Fig. 10. Time series of the direction-coherence ratio for $N = 21$, $\alpha = 0.49$, and $\epsilon = 1.0$.

5. Unstable dimension variability and shadowing breakdown

The main issue to be discussed in this section is the relation between the on–off intermittent transition to synchronization and the breakdown of shadowing of chaotic trajectories which accompanies the loss of hyperbolicity via unstable dimension variability. Continuous shadowability of pseudo-trajectories for a reasonable time-span is a sufficient, albeit not necessary, requirement for numerically generated chaotic trajectories to be valid [22]. In the case of complex systems like a coupled map lattice, with many degrees of freedom and displaying a rich spatio-temporal dynamical behavior, the question of shadowing is of paramount importance. As we shall see, unstable dimension variability is quite common in those systems for practically any coupling strength [60–62]. There are many observable consequences of unstable dimension variability in a chaotic system, like the geometric growth of very small one-step errors in the numerical procedures to obtain trajectories. As a result of that, our confidence in long time averages of dynamical quantities like entropies and dimensions, is questioned [63]. Another consequence of unstable dimension variability in complex systems of the form (1) turns out to be the intermittent transition to synchronization.

In the previous section we have interpreted that the existence of an intermittent transition to synchronization is mediated by an unstable–unstable pair bifurcation occurring in the chaotic attractor lying on the synchronization manifold. This bifurcation marks the onset of unstable dimension variability in the chaotic dynamics, since a periodic orbit, and all its pre-images embedded in the system attractor, lose transversal stability with respect to the synchronization manifold. These transversely unstable orbits form a dense set of repelling tongues and they are responsible for the intermittent bursts of non-synchronization. There remains, however, an infinitely large number of embedded transversely stable periodic and aperiodic orbits, which are ultimately responsible for the existence of the laminar synchronization intervals. For that reason, it has been proposed to call this process an intermittency induced by unstable dimension variability, when the on–off intermittent bursting is followed by violent loss of hyperbolicity in the system dynamics [64].

As the parameter is increased, the number of unstable periodic orbits, that are transversely unstable, also increases. A way to quantify the relative abundance of periodic orbits with a different number of unstable directions is to calculate the corresponding finite-time, or time-n, Lyapunov exponents $\lambda_i(n)$, $i = 1, \cdots N$. They are computed in the same way as the Lyapunov spectrum we discussed in Section 2, but using trajectories of small duration, say $n = 50$ iterations. The usual spectrum is obtained formally as the infinite-time limit of them $\lambda_i = \lim_{n\to\infty} \lambda_i(n)$. Unlike the usual spectrum, where the computed exponents are the same for almost every initial condition (except for a Lebesgue measure zero set), the time-n exponents are generally different for different initial conditions, and they yield a distribution centered at the infinite-time limit.

It has been recognized as a fingerprint of unstable dimension variability in dynamical systems the fluctuating behavior (about zero) of the time-n exponent closest to zero [16] for trajectories belonging to the synchronization manifold $\mathcal{S}$ of the coupled map lattice. The finite-time Lyapunov exponent is computed along a direction transversal to $\mathcal{S}$. A completely synchronized behavior means that $\lambda_1 > 0$ and $\lambda_i \leq 0$ for $i = 2, 3, \ldots$. Hence, the finite-time Lyapunov exponent closest to zero that fluctuates about zero, when $\mathcal{S}$ loses hyperbolicity through unstable dimension variability, is $\lambda_2(n)$. The corresponding eigendirection will be referred to as the transversal direction (even though there are many other transversal directions as well). To understand the reason for this fluctuating behavior, let us consider an initial condition off but very close to the invariant subspace $\mathcal{S}$. Such a chaotic trajectory visits ϵ-neighborhoods of saddles and repellers of the invariant set $\mathcal{S}$. This means that there are time-n segments for which the trajectory is transversely attracting (on average) and others for which it is transversely repelling (also on average) [17].

The fluctuating behavior of the finite-time transversal Lyapunov exponent $\lambda_2(n)$ suggests the usefulness of a probability distribution $P(\lambda_2(x_0, y_0 = 0; n))$ for them, so that $P(\lambda_2)\mathrm{d}\lambda_2$ is the probability that the transversal time-n exponent has a value between λ_2 and $\lambda_2 + \mathrm{d}\lambda_2$ for a given n [18]. Hence, unstable dimension variability implies a positive tail in $P(\lambda_2)$, even though the average time-n exponent, defined as

$$m \equiv < \lambda_2(x_0, y_0 = 0; n) > = \frac{\int_{-\infty}^{+\infty} P(\lambda_2(x_0, y_0 = 0; n))\lambda_2 \mathrm{d}\lambda_2}{\int_{-\infty}^{+\infty} P(\lambda_2(x_0, y_0 = 0; n))\mathrm{d}\lambda_2} = \lambda_\mathrm{T} \qquad (9)$$

may be less than zero. In fact, when m is equal to zero, the negative and positive areas of the distribution are equal and the unstable dimension variability is the most intense (the amount of transversely attracting and repelling contributions nearly counterbalance each other). At this point, the synchronization manifold loses transversal stability as a whole, and the infinite-time transversal exponent vanishes, ($m = \lambda_\mathrm{T} = 0$), characterizing a blowout bifurcation [65].

We can get a numerical approximation for the probability distribution $P(\lambda_2(n))$ by considering a large number of trajectories of length n from initial conditions randomly chosen in the synchronization manifold. In Fig. 12, we show some distributions of time-50 exponents, obtained for different values of the effective range α, which here plays the role of a bifurcation parameter. The critical value for the onset of unstable dimension variability is also the onset of intermittent transition to complete synchronization, at $\alpha = \alpha_\mathrm{c}$, where an unstable–unstable pair bifurcation occurs in the synchronization manifold. Numerically the onset of unstable dimension variability is estimated by computing the value of α for which the fraction of positive finite-time Lyapunov exponents,

$$\phi(n) = \frac{\int_{0}^{+\infty} P(\lambda_2(x_0, y_0 = 0; n))\lambda_2 \mathrm{d}\lambda_2}{\int_{-\infty}^{+\infty} P(\lambda_2(x_0, y_0 = 0; n))\mathrm{d}\lambda_2} \qquad (10)$$

becomes non-zero, yielding the points on the curve $\epsilon_c(\alpha)$ depicted in Fig. 4(b). Hence, for $\alpha < \alpha_\mathrm{c}$, no shadowing breakdown via unstable dimension variability is expected, and the chaotic synchronized trajectories are expected to be adequately shadowed over a longer time interval, which may be long enough for practical purposes (e.g., when computing dimensions and entropies).

The shape of the probability distributions in Fig. 12 is Gaussian-like, with different variances σ^2, according to the value which α takes on. The Gaussian-like nature of $P(\lambda_2(n))$ is already expected on general grounds [18], and the distribution as a whole drifts toward positive values of $\lambda_2(n)$, as α increases. When $\alpha = \alpha^*$, the average $m = \langle\lambda_2(n)\rangle$ crosses zero and has a maximum unstable dimension variability (Fig. 13) since, at this point, $m = 0$, as illustrated by the distribution for $\alpha = 1.14834 \gtrsim \alpha^*$ shown in Fig. 12. Accordingly, the points on the curve $\epsilon^*(\alpha)$ (Fig. 4) were also computed by imposing that $m = 0$, which furnished the same results as those obtained with help of the order parameter $\bar{R}$, thus confirming the relationship between the loss of synchronization and the shadowing breakdown via unstable dimension variability.

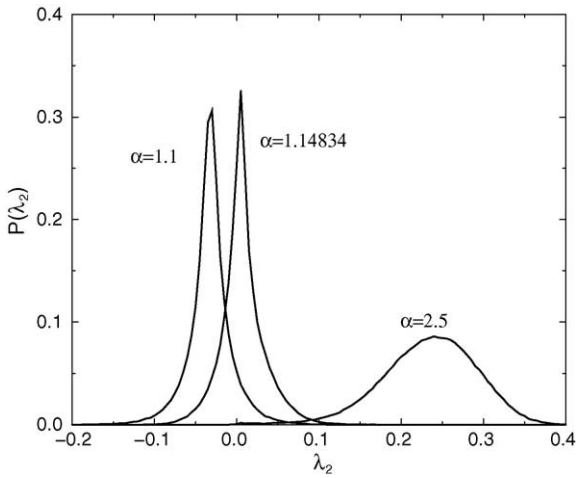

Fig. 12. Distributions of the second (transversal) finite-time Lyapunov exponent for different values of the effective range α, for $\epsilon = 1.0$.

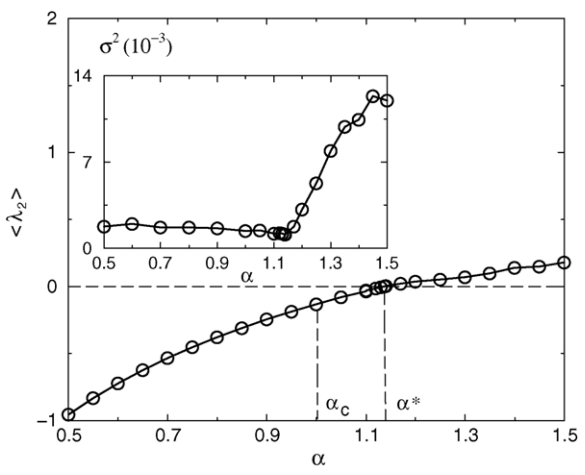

Fig. 13. Average of the second (transversal) finite-time Lyapunov exponent vs. the effective range, for $\epsilon = 1.0$. The inset shows the corresponding variance.

In the vicinity of the point $\alpha = \alpha^*$, the shadowing times can be very short, and the validity of the computed numerical trajectories is doubtful beyond that. There results the time-n exponents (with n greater than the shadowing time), may suffer from similar shadowability problems, when taking individually, as the chaotic trajectories themselves. However, in terms of the numerical diagnostics of unstable dimension variability, we are actually interested in statistical properties of the time-n exponents, as their averages and variances, but for n very small. The former yields the point where unstable dimension variability is the most intense, at the a blowout instability, whereas the latter can be used to estimate shadowing times [66]. On the other hand, in some physically relevant cases, statistical quantities like these have been found to be meaningful despite unstable dimension variability [67].

For $\alpha > \alpha^*$, the relative number of positive time-n exponents increases and we progressively return to a situation where unstable dimension variability is less pronounced, and better shadowing properties are expected. For example, when $\alpha = 2.5$, Fig. 12 indicates that the second time-n exponents is positive for most initial conditions. This means that, even though the lattice trajectories are far from being complete synchronized, they are nonetheless better shadowed than before. Fig. 13 also depicts the variance of the distributions, showing that it is roughly constant until α reaches the blowout value α^*, after that the distribution broadens up and the variance increases.

The relation between unstable dimension variability and shadowing breakdown can be put on a more quantitative ground. There was shown that the shadowing time, or the time-span for which a numerical trajectory is continuously shadowed by a true chaotic trajectory, can be estimated as [66] $\langle\tau\rangle \sim q^{-h(m)}$, where q is the precision of the arithmetics used in numerical computation (number of precision digits) of chaotic trajectories, and

$$h(m) \equiv \frac{2|m|}{\sigma_1^2} \tag{11}$$

is the so-called *hyperbolicity coefficient* [63], σ_1^2 being the variance of the distribution of the time-1 Lyapunov exponent closest to zero ($P(\lambda_2(1))$). The latter is related to the variance of the corresponding time-n exponent by $\sigma_n^2 = n\sigma_1^2$. There results that, if $m = 0$, the shadowing time has a minimum value, such that the effect of unstable dimension variability is so intense that we do not expect shadowing for more than thousand iterations of the dynamical process.

6. Conclusions

In this paper we pursued the close correspondence between shadowing breakdown via unstable dimension variability and the intermittent transition to synchronization in a complex system comprised of a coupled map lattice with variable range coupling. A tunable parameter allows us to pass continuously from a local (nearest-neighbor) to a global (mean field) coupling. The existence of a transition to synchronization as this variable range is swept over its interval is a well-established fact, but in this paper we focused on the behavior near criticality.

The intermittent transition studied is akin to the on–off intermittency, and both share common properties, since there is an invariant subspace in the coupled map lattice, which is the synchronization manifold. The distribution of the laminar regions reveals a power-law scaling with the interval length, having a 3/2 universal exponent characterizing on–off intermittency, and also presents a shoulder with an exponential decay for large intervals, as expected if noise is added to the system. In our case, the role of noise is played by the chaotic fluctuations due to bursting in different parts of the lattice, through the coupling term added to each map in the lattice.

The transversal stability properties of the synchronization manifold explain the bursting of non-synchronization which characterizes the abovementioned transition. If there are some, but not all, periodic orbits embedded in the synchronization manifold which do not have transversal stability, a trajectory starting off but very close to this manifold will experience at first a laminar behavior, but the existence of transversely unstable orbits will eventually make this trajectory to burst away. The remaining transversely stable periodic (and aperiodic) orbits will push the trajectory back to the synchronization manifold.

We have used a simpler two-dimensional map with an invariant subspace to argue that the transition to synchronization is mediated by an unstable–unstable pair

bifurcation. On the other hand, this bifurcation also marks the loss of hyperbolicity of the chaotic attractor embedded in the synchronization manifold by means of unstable dimension variability. The synchronization transition can then be understood by considering the statistical properties of the finite-time Lyapunov exponent in the direction transversal to the synchronization manifold. In particular, we have determined the situation for which the loss of shadowing via unstable dimension variability is more intense, namely, when the synchronization, manifold as a whole, loses transversal stability. Similar properties were found to hold if we consider the behavior of the direction coherence of the lattice sites.

While our discussion was based on a specific coupled map lattice, we argue that the general features observed are rather typical for complex systems presenting regular and chaotic behavior in space and time. The existence of more than one positive Lyapunov exponent when a system parameter, like the coupling strength, is varied, indicates that the synchronization manifold (when it exists) has lost transversal stability. Hence, the connection between shadowing breakdown and intermittent transition to synchronization is a common feature of complex systems.

Acknowledgements

This work was made possible through partial financial support from the following Brazilian research agencies: FAPESP, CNPq, and CAPES. C.G. was also supported by A.V. Humboldt Foundation (Germany). We acknoledge C. Anteneodo for useful suggestions.

References

[1] P. Grassberger, F. Ramos-Gomez (Eds.), Fifth Mexican School on Statistical Mechanics, World Scientific, Singapore, 1991, p. 57.
[2] K. Kaneko, K. Kaneko (Eds.), Theory and Applications of Coupled Map Lattices, Wiley, Chichester, 1993.
[3] R. Badii, A. Politi, Complexity: Hierarchical Structures and Scaling in Physics, Cambridge Nonlinear Science Series, vol. 6, Cambridge University Press, 1997.
[4] J. Kurths, A. Voss, P. Saparin, H.J. Kleiner, N. Wessel, Chaos 5 (1995) 88.
[5] H. Fujisaka, T. Yamada, Prog. Theor. Phys. 69 (1983) 32.
[6] L.M. Pecora, T.L. Carroll, Phys. Rev. Lett. 64 (1990) 821.
[7] A. Pikovsky, M. Rosemblum, J. Kurths, Synchronization—A Universal Concept in Nonlinear Sciences, Cambridge University Press, 2001.
[8] S. Bocalletti, J. Kurths, G. Osipov, D.L. Valladares, C.S. Zhou, Phys. Reports 366 (2002) 1.
[9] E. Ott, P. So, E. Barreto, T. Antonsen, Physica D 173 (2002) 29.
[10] L.M. Pecora, T.L. Carroll, G.A. Johnson, D.J. Mar, J.F. Heagy, Chaos 7 (1997) 520.
[11] A.M. Batista, S.E. de S. Pinto, R.L. Viana, S.R. Lopes, Phys. Rev. E 65 (2002) 056209.
[12] J.F. Heagy, N. Platt, S.M. Hammel, Phys. Rev. E 49 (1994) 1140.
[13] P. Ashwin, J. Buescu, I. Stewart, Phys. Lett. A 193 (1994) 126.
[14] P. Ashwin, J. Buescu, I. Stewart, Nonlinearity 9 (1996) 703.
[15] R. Abraham, S. Smale, Proc. Symp. Pure Math. (AMS) 14 (1970) 5.
[16] S.P. Dawson, C. Grebogi, T. Sauer, J.A. Yorke, Phys. Rev. Lett. 73 (1994) 1927.
[17] R.L. Viana, S.E. de S. Pinto, J.R.R. Barbosa, C. Grebogi, Int. J. Bifurcat. Chaos 13 (2003) 1.
[18] E.J. Kostelich, I. Kan, C. Grebogi, E. Ott, J.A. Yorke, Physica D 109 (1997) 81.
[19] D.V. Anosov, Proc. Steklov Inst. Math. 90 (1967) 1.
[20] R. Bowen, J. Diff. Eq. 18 (1975) 333.
[21] C. Grebogi, S. Hammel, J.A. Yorke, Bull. Am. Math. Soc. 19 (1988) 465.
[22] C. Grebogi, L. Poon, T. Sauer, J. A. Yorke, D. Auerbach, Shadowability of chaotic dynamical systems, in: Handbook of Dynamical Systems, vol. 2, Fiedler, North-Holland, Amsterdam, 2002, pp. 313–344.
[23] S.C. Venkataramani, T.M. Antonsen Jr., E. Ott, J.C. Sommerer, Phys. Lett. A 207 (1995) 173.
[24] G. Paladin, A. Vulpiani, J. Phys. A 25 (1994) 4511.
[25] A. Torcini, S. Lepri, Phys. Rev. E 55 (1997) R3805.
[26] S.E. de S. Pinto, R.L. Viana, Phys. Rev. E 61 (2000) 5154.
[27] H. Nozawa, Chaos 2 (1992) 377.
[28] S. Ishii, M. Sato, Physica D 121 (1998) 344.
[29] P.M. Gade, C.-K. Hu, Phys. Rev. E 60 (1999) 4966.
[30] Y. Kuramoto, H. Nakao, Physica D 103 (1997) 294.
[31] Y. Kuramoto, D. Battogtokh, H. Nakao, Phys. Rev. Lett. 81 (1998) 3543.
[32] S. Raghavachari, J.A. Glazier, Phys. Rev. Lett. 74 (1995) 3297.
[33] K. Kaneko, Physica D 23 (1986) 436.
[34] K. Kaneko, Physica D 34 (1989) 1.
[35] K. Kaneko, Physica D 41 (1990) 137.
[36] T. Shimada, K. Kikuchi, Phys. Rev. E 62 (2000) 3489.
[37] C. Anteneodo, S.E. de S. Pinto, A.M. Batista, R.L. Viana, Phys. Rev. E 68 (2003) 045202(R); C. Anteneodo, A.M. Batista, R.L. Viana, Phys. Lett. A 326 (2004) 227.
[38] K. Kaneko, Physica D 37 (1989) 60.
[39] K. Wiesenfeld, P. Colet, S.H. Strogatz, Phys. Rev. Lett. 76 (1996) 404.
[40] K. Wiesenfeld, P. Colet, S.H. Strogatz, Phys. Rev. E 57 (1998) 1563.
[41] D. Tsygankov, K. Wiesenfeld, Phys. Rev. E 66 (2002) 036215.

[42] S.H. Strogatz, Nonlinear Dynamics and Chaos, Addison Wesley, 1984.
[43] D.J. DeShazer, R. Breban, E. Ott, R. Roy, Phys. Rev. Lett. 87 (2001) 044101.
[44] C. Schäfer, M.G. Rosenblum, H.-H. Abel, J. Kurths, Phys. Rev. E 60 (1999) 857.
[45] Y. Kuramoto, Chemical Oscillations, Waves, and Turbulence, Springer Verlag, Berlin, 1984.
[46] R.L. Viana, C. Grebogi, S.E. da S. Pinto, S.R. Lopes, A.M. Batista, J. Kurths, Phys. Rev. E 68 (2003) 067204.
[47] F. Schmüser, W. Just, H. Kantz, Phys. Rev. E 61 (2000) 3675.
[48] A. Pikowsky, G. Osipov, M. Rosenblum, M. Zaks, J. Kurths, Phys. Rev. Lett. 79 (1997) 47.
[49] Y.-C. Lai, C. Grebogi, J.A. Yorke, S.C. Venkataramani, Phys. Rev. Lett. 77 (1996) 55.
[50] C. Grebogi, E. Ott, J.A. Yorke, Phys. Rev. Lett. 50 (1983) 935.
[51] C. Grebogi, E. Ott, J.A. Yorke, Ergod. Th. Dynam. Sys. 5 (1985) 341.
[52] R.L. Viana, C. Grebogi, Int. J. Bifurcat. Chaos 11 (2001) 2689.
[53] E. Covas, P. Ashwin, R. Tavakol, Phys. Rev. E 56 (1997) 6451; Y. Do, Y.-C. Lai, Z. Liu, E.J. Kostelich, Phys. Rev. E 67 (2003) 035202(R).
[54] C. Zhou, J. Kurths, Phys. Rev. Lett. 88 (2002) 230602.
[55] C. Zhou, C.-H. Lai, Physica D 135 (2000) 1.
[56] G.V. Osipov, A.S. Pikowsky, M.G. Rosenblum, J. Kurths, Phys. Rev. E 55 (1997) 2353.
[57] B. Hu, Z. Liu, Phys. Rev. E 62 (2000) 2114.
[58] W. Wang, Z. Liu, B. Hu, Phys. Rev. Lett. 84 (2000) 261.
[59] W. Wang, Z. Liu, B. Hu, Phys. Rev. E 55 (1997) 2353.
[60] Y.-C. Lai, C. Grebogi, Phys. Rev. Lett. 82 (1999) 4803.
[61] Y.-C. Lai, C. Grebogi, J. Bifurcat. Chaos 10 (2000) 683.
[62] Y.-C. Lai, D. Lerner, K. Williams, C. Grebogi, Phys. Rev. E 60 (1999) 5445.
[63] T.D. Sauer, Phys. Rev. E 65 (2002) 036220.
[64] R.L. Viana, S.E. de S. Pinto, C. Grebogi, Phys. Rev. E 66 (2002) 046213.
[65] E. Ott, J.C. Sommerer, Phys. Rev. Lett. 71 (1993) 4134.
[66] T. Sauer, C. Grebogi, J.A. Yorke, Phys. Rev. Lett. 79 (1997) 59.
[67] Y.-C. Lai, C. Grebogi, J. Kurths, Phys. Rev. E 59 (1999) 2907.